ISSN 1063-7745, Crystallography Reports, 2019, Vol. 64, No. 7, pp. 1023–1029. © Pleiades Publishing, Inc., 2019.

STRUCTURE OF ORGANIC COMPOUNDS

Hydrothermal Synthesis and Physicochemical Characterization of Organic-Inorganic Isopolyoxomolybdate-Based Hybrid $(C_6N_6)_4[H_4Mo_8O_{26}]$

M. M. Ftini[a,*], A. Chaabani[a], and T. Boubaker[a]

[a] *Department of Chemistry, University of Monastir, Monastir, Tunisia*

** e-mail: mohamedmongi@yahoo.fr*

Received January 3, 2018; revised March 15, 2019; accepted April 1, 2019

Abstract—A novel polyoxomolybdate-based organic-inorganic hybrid compound, $(C_6H_6)_4[H_4Mo_8O_{26}]$, has been synthesized hydrothermally and characterized structurally by the elemental analysis, single crystal X-ray diffraction, thermogravimetric analysis, infrared and ultraviolet–visible spectroscopies, and cyclic voltammetry. Crystallographic data for the compound are: triclinic system, space group $P\bar{1}$, unit cell parameters a = 9.605(2) Å, b = 9.991(3) Å, c = 10.718(3) Å, $\alpha = 83.75(2)°$, $\beta = 76.45(3)°$, $\gamma = 69.07(3)°$, $Z = 1$. The crystal consists of the clusters β-$[Mo_8O_{26}]^{4-}$ and four organic molecules C_6H_6. Isopolymolybdate anions are connected with the organic molecules via a complex hydrogen-bonded network, which generate a three-dimensional framework.

DOI: 10.1134/S1063774519070058

INTRODUCTION

Polyoxometalates (**POM**s) are oxo-metal clusters, in which the metal element M is often in its highest oxidation state ($M = W^{VI}$, Mo^{VI}, V^{V} et al.). The class of POMs can be subdivided in isopolyanions and heteropolyanions. The first class is formed only by a metal element and oxygen ligands. The well-known examples are hexa-metallate $[M_6O_{19}]^{2-}$ (M = Mo, W), hepta-metallate $[Mo_7O_{24}]^{6-}$, and octa-metallate $[Mo_8O_{26}]^{4-}$ ions. The second class contains an additional heteroelement X, which can either be from the main groups or the d-block. The known examples of heteropolyanions are: the Keggin ion, $[XM_{12}O_{40}]^{n-}$ the Anderson-Evans ion, $[XM_6O_{24}]^{n-}$; the Wells-Dawson ion, $[X_2M_{18}O_{62}]^{n-}$.

The POM-based organic–inorganic hybrid compounds have attracted a great interest in recent years due to their theoretical and practical applications in catalysis [1–6], medicine [7–11], optics and magnetism [12–20], nanotechnologies [21, 22], and photoluminescence area [23–27]. A strategy is to substitute an inorganic cation such as H^+, Na^+, K^+, and NH_4^+ by organic molecules, which will act not only as a charge compensators but also play an important role in the polymerization of the POMs via Van der Waals, hydrogen bonding and/or electrostatic interactions of conventional O–H···O, C···H, and N–H···O motifs [28, 29], leading to obtain original hybrid materials.

The octamolybdate family, $[Mo_8O_{26}]^{4-}$, has attracted a great interest due to its different structural modifications in solid state: eight isomeric forms, α, β, γ, θ, δ, ε, ζ, and η, have been prepared, they differ in types of polyhedra that fuse to form a cluster and a bonding between polyhedra [30–32]. The octamolybdate isomers could be crystallized through organic cations, such as $(HDBU)_3(NH_4)[\beta\text{-}Mo_8O_{26}] \cdot H_2O$ [33], $(HDBU)_4[\delta\text{-}Mo_8O_{26}]$ [33], $(C_{10}H_{10}N_2)_2(C_{10}H_8N_2)[Mo_8O_{26}] \cdot 2H_2O$ [34], and $(C_4H_{14}N_2)_2[Mo_8O_{26}] \cdot 2H_2O$ [35], or through metal-ligand cations, such as $[\{Cu(tpdoen)\}_2][\alpha\text{-}Mo_8O_{26}] \cdot 3H_2O$ [36], $[\{Ni(tpoen)\}_2(\beta\text{-}Mo_8O_{26})] \cdot 5H_2O$ [36], $\{Co(phen)_3\}_2[Mo_6O_{19}][Mo_8O_{26}] \cdot 2H_2O$ [37], $[\{Cu_2(tpyrpyz)\}_2\{\zeta\text{-}Mo_8O_{26}\}] \cdot 7H_2O$ [38], and $[Fe(tpyprz)_2]_2[Mo_8O_{26}] \cdot 3.7H_2O$ [39].

In this paper, we report the hydrothermal synthesis, molecular structure, and physical properties of polyoxomolybdate-based organic-inorganic hybrid, $(C_6H_6)_4[H_4Mo_8O_{26}]$.

EXPERIMENTAL

Synthesis

The compound, $(C_6H_6)_4[H_4Mo_8O_{26}]$, was prepared via the hydrothermal synthesis in a 25 mL Teflon-lined reactor. Sodium molybdate dihydrate $Na_2Mo_2O_4 \cdot 2H_2O$ (1.452 g, 6 mmol) was dissolved in 10 ml of water, after addition of aniline (0.2 mL, 2.2 mmol), the pH value was adjusted to 2.7 by adding a concentrated hydrochloric acid. The resulting mix-

Table 1. Crystallographic characteristics and the X-ray-data collection and structure-refinement parameters for the $(C_6H_6)_4[H_4Mo_8O_{26}]$

System, sp. gr., Z	Triclinic, $P\bar{1}$, 1
a, b, c, Å	9.605(2), 9.991(3), 10.718(3)
α, β, γ, deg	83.75(2), 76.45(3), 69.07(3)
V, Å^3	933.6(3)
D_x, g cm^{-3}	2.661
Radiation, λ, Å	Mo $K\alpha$, 0.71073
μ, mm^{-1}	2.692
T, K	293(2)
Sample size, mm	0.40 × 0.30 × 0.20
Diffractometer	Enraf-Nonius CAD-4
Scan mode	ω–2θ
Absorption correction, T_{min}, T_{max}	Psi-scans, 0.392, 0.593
θ_{max}, deg	25.349
h, k, l ranges	$-11 \le h \le 12$, $-12 \le k \le 12$, $0 \le l \le 13$
Number of reflections:	
measured/unique ($N1$),	5342/3969
R_{int}/with $I > 2\sigma(I)$ ($N2$)	0.033/3503
Refinement method	Full-matrix least-squares
Number of refined parameters	301
R_1/wR_2 relative to $N1$	0.0473/0.01007
R_1/wR_2 relative to $N2$	0.0403/0.0975
S	1.0175
$\Delta\rho_{max}/\Delta\rho_{min}$, e/Å^3	1.12/–2.07

ture was stirred at room temperature until the mixture became homogeneous, then it was transferred and sealed in a Teflon-lined autoclave, which was heated at 120°C for 72 h. After slow cooling to room temperature the crystalline product was filtered, washed with distilled water, and dried at ambient temperature.

Single-Crystal X-Ray Diffraction

A suitable single crystal of the title compound with dimensions 0.40 × 0.30 × 0.20 mm was mounted on a glass fiber. Data were collected at 293 K on a Enraf-Nonius CAD-4 diffractometer with a MoK_α (λ = 0.71073 Å) monochromated radiation. The data were corrected using an empirical absorption correction (ψ_{scans}) [40]. The structure was solved by direct methods using SHELXS-97 program [41] and refined by full-matrix least-squares based on F^2 using SHELXL-97 program [41] included in the software package WinGX [42]. All non-hydrogen atoms were directly located from difference Fourier maps and refined with anisotropic displacement parameter. Hydrogen atoms were located from difference Fourier maps calculated from successive least-squares refinements, these atoms were added in idealized positions and refined in subsequent refinement cycles with an isotropic displacement parameter fixed at $1.2U_{eq}$ (Å^2) of the parent atoms. The crystal data and structure refinement parameters for the title compound are given in Table 1. The selected bond lengths are listed in Table 2.

The crystallographic data for the title compound were deposited with the Cambridge Crystallographic Data Centre (CCDC number 1469694). These data can be obtained free of charge via http://www.ccdc.cam.ac.uk.

Physical Measurements

Fourier transform infrared (**FT-IR**) spectra were recorded in the 4000-400 cm^{-1} range on a Perkin Elmer Spectrum 65 FT IR Spectrometer.

Thermogravimetric analysis (**TG**) and differential thermal analyses (**DTA**) were carried out simultaneously using a SETARAM TG-DTA92 instrument. The sample mass of 9 mg was placed in a platinum crucible heated from 25 to 600°C in a dynamic N_2 atmosphere. The heating rate was 10°C min^{-1}.

The ultraviolet–visible (**UV**) absorption behavior of the title compound was analyzed in the 200–400 nm range using an aqueous solution (2×10^{-3} M) with a Perkin-Elmer Lambda 650 spectrophotometer.

The electrochemical behavior was studied by cyclic voltammetry in 0.2 M H_2SO_4 aqueous solutions at different scan rates in the potential range from 0 to 1 V. Platinum electrodes were used as the working electrode and counter electrode, the reference electrode was an Ag/AgCl (sturated KCl) electrode.

RESULTS AND DISCUSSION

Crystal Structure

Single-crystal X-ray diffraction analysis reveals that the title compound is constructed of β-$[Mo_8O_{26}]^{4-}$ and four organic molecules linked via hydrogen bonding interaction. The β-$[Mo_8O_{26}]^{4-}$ anion consists of eight distorted edge-sharing $[MoO_6]$ octahedra (Fig. 1). Due to different coordination modes of oxygen atoms in polyanion unit, the Mo–O bond lengths can be classified into four categories: (I) Mo–Ot bonds, where Ot is the terminal oxygen atom O2, O3, O5, O9, O10, O12, O13, O2$^{\#1}$, O3$^{\#1}$, O5$^{\#1}$, O9$^{\#1}$, O10$^{\#1}$, O12$^{\#1}$, O13$^{\#1}$, 1.685–1.722 Å; (II) Mo–Ob bonds, where Ob is the twofold-coordinated oxygen atom O7, O8, O11, O7$^{\#1}$, O8$^{\#1}$, O11$^{\#1}$, 1.749–2.289 Å; (III) Mo–Oc bonds, where Oc is threefold-coordinated oxygen atom O1, O4, O1$^{\#1}$, O4$^{\#1}$, 1.949–2.366 Å; (IV) Mo–Op bonds, where Op is the pentafold-coordinated oxygen atom O6, O6$^{\#1}$, 2.135–2.517 Å (Table 2).

Table 2. Selected bond lengths *d* (Å) and angle limits (deg) for the $(C_6H_6)_4[H_4Mo_8O_{26}]$

Bonds	*d*, Å	Bonds	*d*, Å
Mo1–O1	1.949(5)	Mo3–O1$^{\#1}$	2.366(2)
Mo1–O3	1.711(6)	Mo3–O2	1.721(6)
Mo1–O4	1.956(5)	Mo3–O4	1.999(6)
Mo1–O6	2.135(5)	Mo3–O6	2.336(5)
Mo1–O6$^{\#1}$	2.380(5)	Mo3–O8	1.889(6)
Mo1–O11	1.749(6)	Mo3–O9	1.696(6)
Mo2–O1	1.996(5)	Mo4–O5	1.722(7)
Mo2–O4$^{\#1}$	2.357(5)	Mo4–O6	2.517(5)
Mo2–O6	2.327(5)	Mo4–O7	1.929(6)
Mo2–O7	1.890(6)	Mo4–O8	1.927(6)
Mo2–O10	1.702(6)	Mo4–O11$^{\#1}$	2.289(6)
Mo2–O13	1.708(6)	Mo4–O12	1.685(6)
Polyhedra	Angle limits	Polyhedra	Angle limits
$Mo1O_6$	75.71(2)–174.83(2)	$Mo3O_6$	71.25(1)–158.52(2)
$Mo2O_6$	71.78(2)–163.22(2)	$Mo4O_6$	68.86(1)–164.89(2)

Symmetry code: #1) $-x, -y, -z$.

The +6 oxidation state of Mo atoms was confirmed by the bond valence sum (**BVS**) calculations [43], according to which the valence sum from Mo1 to Mo4 is 6.085, 5.953, 5.909, and 5.928, respectively, the average value being 5.969, which is consistent with that expected for Mo in +6 oxidation state. According to the results of the bond valence sum for all oxygen atoms in the cluster anion, we presume that the H^+ ions for the balancing charge may be bonded to the terminal oxygen, O2 and O2$^{\#1}$ (BVS = 1.556), and the pentafold-coordinated oxygen, O6 and O6$^{\#1}$ (BVS = 1.456), as their BVS values are smaller than those of the other oxygen atoms yielding to the $[H_4Mo_8O_{26}]$ cluster. The organic molecules C_6H_6 are in two crys-

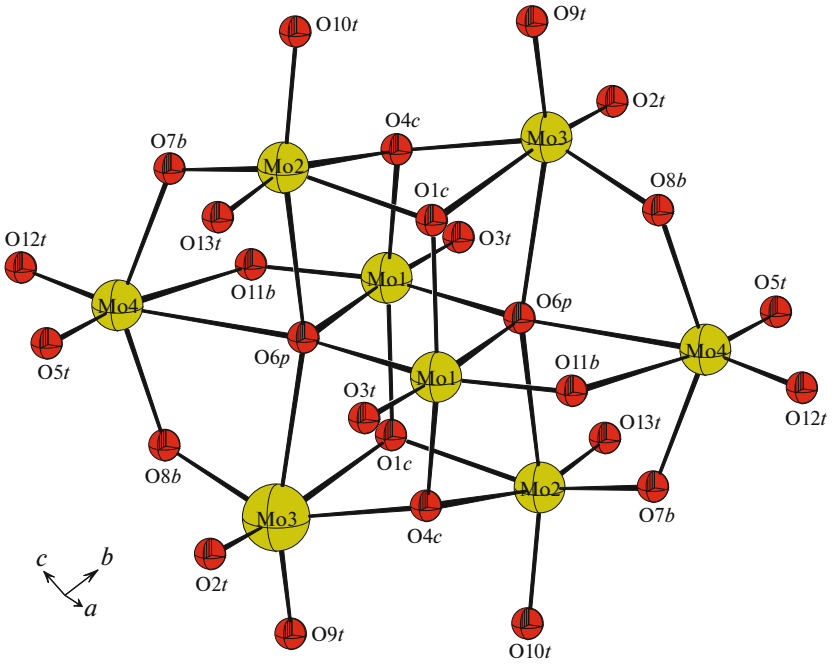

Fig. 1. Ball-and-stick representation of the octamolybdate β-$[Mo_8O_{26}]^{4-}$ cluster anion.

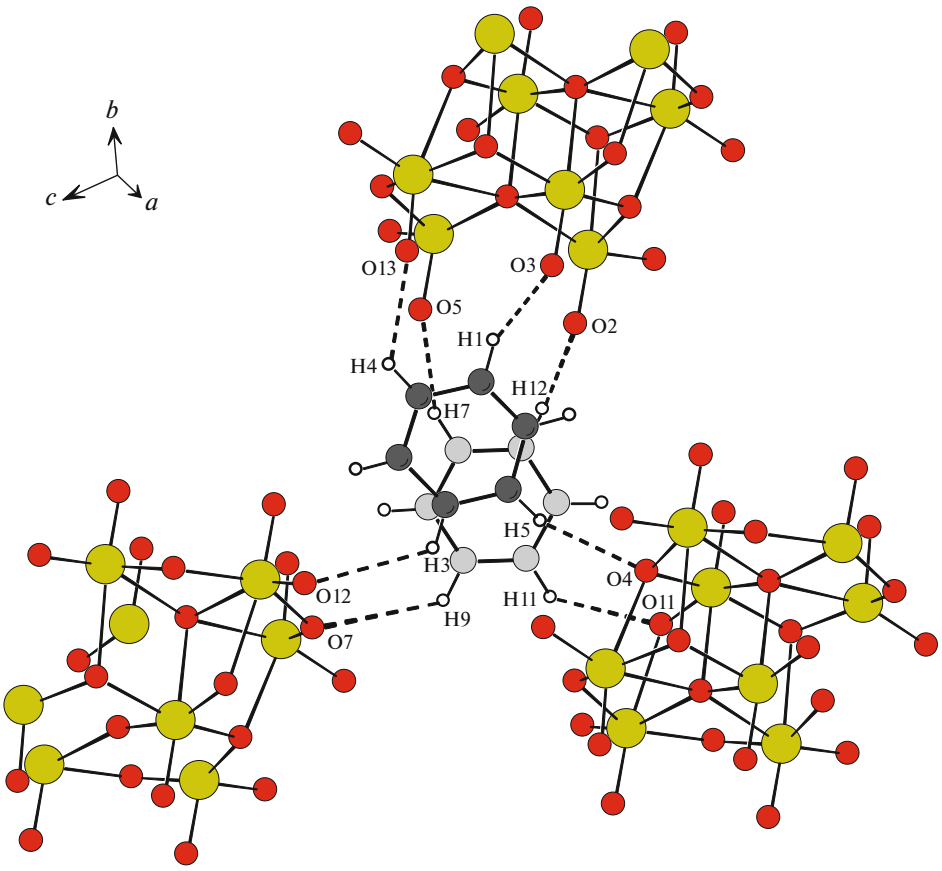

Fig. 2. Representation of the association mode of the organic molecules and the β-octamolybdate clusters showing the hydrogen bonding interactions.

tallographically independent sites, which can be named as *M*1 and *M*2. They connect to the clusters by a complex network of hydrogen interactions. The molecules *M*1 and *M*2 are interlinked with three neighboring clusters via hydrogen interactions (Fig. 2). The first cluster shares two oxygen atoms O2 and O5 with *M*1, the bond lengths are C12–H12···O2 = 2.121 Å and C7–H7···O5 = 2.207 Å, and it also shares two other oxygen atoms O3 and O13 with the organic molecule *M*2, the bond lengths are C1–H1···O3 = 1.982 Å, C4–H4···O13 = 2.281 Å. The second cluster is hydrogen bonded to *M*1 via C5–H5···O4 and to *M*2 via C11–H11···O11, the hydrogen bond lengths are 2.422 and 2.491 Å, respectively. The third cluster is connected to the organic molecule *M*1 by sharing its oxygen atom O7, bond length is 2.940 Å, and connected to *M*2 by sharing its oxygen atom O12, bond length is 2.745 Å. The important hydrogen bond interactions observed are listed in Table 3. This arrangement leads to a two-dimensional structure parallel to the plane (111). The three-dimensional structure of title compound is made up by a stack of these identical layers following a stack of *ABAB*-type. The hydrogen bonding interactions exist also between two successive two-dimensional layers (Fig. 3), the organic molecule of the first layer is connected to the cluster of the second layer via hydrogen interactions C2–H2···O9 and C4–H4···O10 with bond lengths 2.701 and 2.343 Å, respectively.

Table 3. Selected hydrogen-bond geometry (Å, deg) for the $(C_6H_6)_4[H_4Mo_8O_{26}]$

D–H···*A*	*D*–H, Å	H···*A*, Å	*D*···*A*, Å	*D*–H···*A*, deg
C1–H1···O3	0.920	1.982	2.864(2)	157
C2–H2···O9	0.924	2.701	3.510(5)	164.9
C3–H3···O12	0.928	2.745	3.317(3)	120.2
C4–H4···O10	0.924	2.343	3.035(2)	131
C4–H4···O13	0.924	2.281	3.049(2)	127
C5–H5···O4	0.922	2.422	3.319(2)	159
C7–H7···O5	0.922	2.207	3.060(2)	153
C9–H9···O7	0.927	2.940	3.524(2)	122.3
C11–H11···O11	0.931	2.491	3.211(2)	133
C12–H12···O2	0.923	2.121	3.010(2)	159

D = donor, *A* = acceptor.

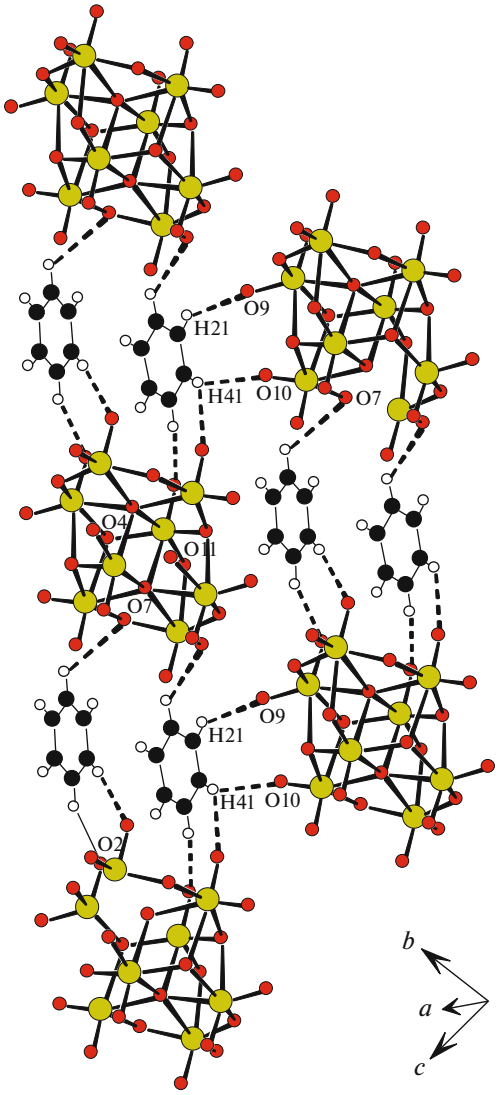

Fig. 3. A view of hydrogen bonding interactions between two 2-dimensional layers in the structure of $(C_6H_6)_4[H_4Mo_8O_{26}]$.

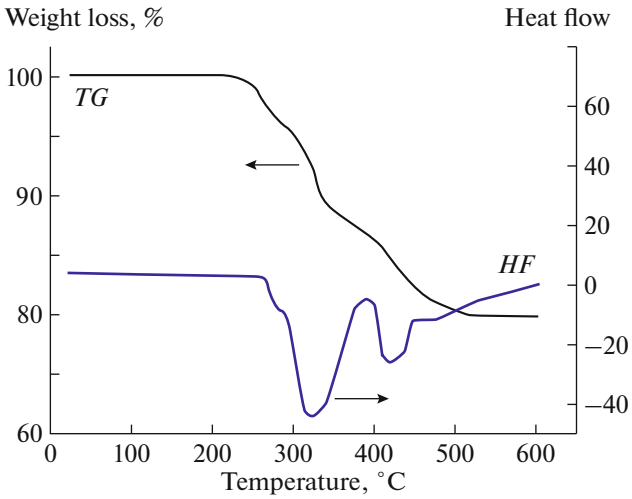

Fig. 4. Thermogravimetric and differential thermal curves of the compound $(C_6H_6)_4[H_4Mo_8O_{26}]$.

Infrared Spectroscopy

The IR spectrum of the title compound shows the characteristic vibrational peak similar to that known for octamolybdate cluster anions. The series of bands in the range of 592–422 cm^{-1} are attributed to the (Mo–O–Mo) vibrations. Bands at 950, 872, and 785 cm^{-1} are assigned to the terminal Mo=O stretching. There are some characteristic bands for the organic molecules at 1382 and 1468 cm^{-1}, which can be ascribed to the aromatic (C=C) vibration. Bands at 2876 and 2963 cm^{-1} are attributed to the characteristic (C–H) aromatic vibration.

Thermogravimetric and Differential Thermal Analyses

The TG curve exhibits a two-step of mass loss in the temperature range from 220 to 500°C (Fig. 4). It can be observed that the experimental result of TG analysis (21.1%) is in agreement with the results of structure determination and the calculated value (20.8%).

The DTA curve shows that two mass losses are endothermic. The first loss display a weight loss of 10.9% (calculated value, 10.4%) occurring from 220 to 350°C corresponding to the loss of two organic molecules C_6H_6. The second weight loss of 10.2% occurs between 350 and 500°C, corresponding to the removal of two other organic molecules (calculated value, 10.4%).

Ultraviolet–Visible Spectroscopy

The UV spectrum of the compound exhibits an absorption peak at 216 nm (Fig. 5), ascribed to the ligand-to-metal charge transfer (**LMCT**) from terminal oxygen atom to the molybdenum center ($O_t \rightarrow Mo$), where the nonbonding electrons localized over the oxygen atoms in the highest occupied molecular orbital (**HOMO**) are transferred to the lowest unoccupied molecular orbital (**LUMO**) of the molybdenum atoms. The absorption onset of the title compound was about 262 nm, indicating an optical energy gap (E_g) of 4.7 eV and the absorption coefficient ε of 9864 mol^{-1} L cm^{-1}.

Electrochemical Behavior

The cyclic voltammogram of the compound $(C_6H_6)_4[H_4Mo_8O_{26}]$ recorded at different scan rates (Fig. 6) shows one reversible redox wave, corresponding to the redox couple $Mo^{VI/V}$ in the cluster structure. The mean peak potential is $E_{1/2} = (Epa + Epc)/2 =$ 607 mV (scan rate: 200 mV s^{-1}). Moreover, the cathodic peak potentials shift toward the negative

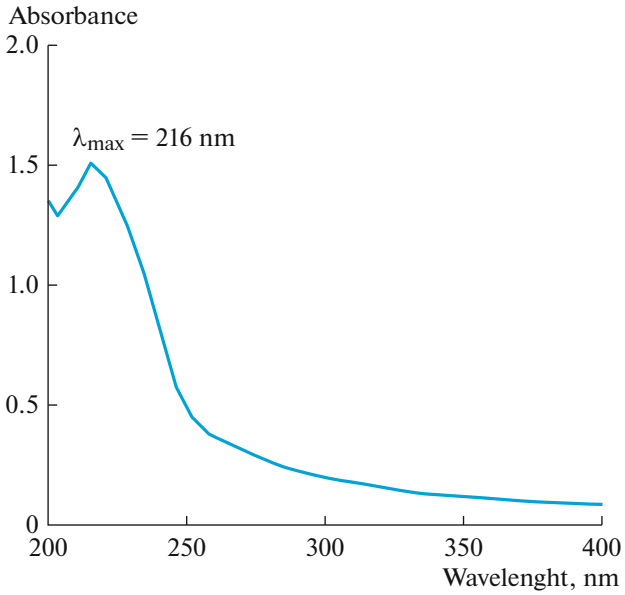

Fig. 5. Ultraviolet–visible absorption spectrum of the compound $(C_6H_6)_4[H_4Mo_8O_{26}]$.

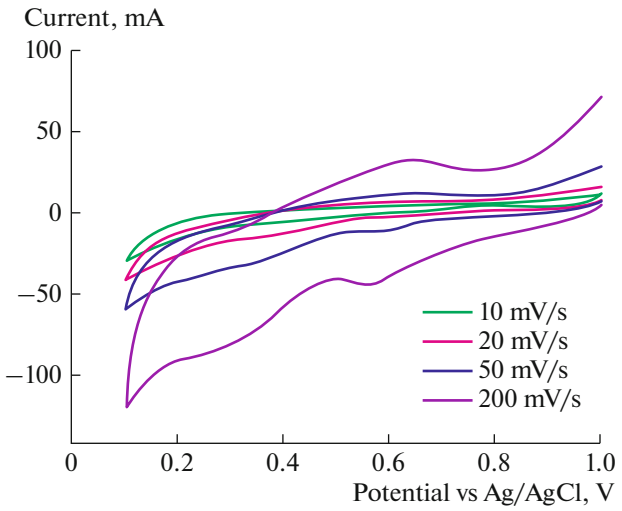

Fig. 6. Cyclic voltammograms of $(C_6H_6)_4[H_4Mo_8O_{26}]$ in H_2SO_4 at different scan rates: 10, 20, 50, 200 mV s^{-1}.

direction and the corresponding anodic peak potentials shift to the positive direction with increasing scan rates. The peak currents are proportional to the square of the scan rates which indicate that the redox process on the electrode is diffusion-controlled.

CONCLUSIONS

In this study, we have hydrothermally-synthesized an organic-inorganic compound $(C_6H_6)_4[H_4Mo_8O_{26}]$ (space group $P\bar{1}$) consisting of β-$[Mo_8O_{26}]^{4-}$ clusters linked by aromatic organic molecule C_6H_6 in a two-dimensional network parallel to the plane (111) via the hydrogen-bonding interactions. The three-dimensional network is made up by a stack of these identical layers following a stack of *ABAB*-type via hydrogen-bonding interactions.

The synthesized compound was characterized by some physicochemical methods. The electrochemical behavior has revealed that the organic-inorganic hybrid polyoxomolybdate exhibits a reversible reduction wave corresponding to the $Mo^{VI/V}$ system. It can be used in modified electrodes to study some electrochemical applications and catalyzed reactions. The ultraviolet–visible spectra of the title compound in aqueous solution display an absorption peaks, appearing at 216 nm, which can be attributed to the charge transfer $p\pi(O_t) \rightarrow d\pi^*(Mo)$. According to the thermogravimetric analysis, the whole weight loss (21.1%) is consistent with the calculated value (20.8%).

REFERENCES

1. B. S. Jaynes and C. L. Hill, J. Am. Chem. Soc. **115**, 12212 (1993).
2. Z. Zheng and C. L. Hill, Chem. Commun. **6**, 2467 (1998).
3. F. Yu, Y. X. Long, Y. P. Ren, et al., Dalton Trans. **39**, 7588 (2010).
4. F. Yu, X.-J. Kong, Y.-Y. Zheng, et al., Dalton Trans. **43**, 9503 (2009).
5. T. Okuhara, N. Mizuno, and M. Misono, Appl. Catal. **222**, 63 (2001).
6. C. Jahier and S. Nlate, Eur. J. Inorg. Chem. **5**, 833 (2012).
7. G. Geisberger, E. B. Gyenge, D. Hinger, et al., Dalton Trans. **42**, 9914 (2013).
8. J. Wang, X. Mi, H. Guan, et al., Chem. Commun. **47**, 2940 (2011).
9. D. A. Judd, J. H. Nettles, N. Nevins, et al., J. Am. Chem. Soc. **123**, 886 (2001).
10. G. Hungerford, F. Hussain, G. R. Patzke, and M. Green, Phys. Chem. Chem. Phys. **12**, 7266 (2010).
11. A. Bijelic, C. Molitor, S. G. Mauracher, et al., ChemBioChem **16**, 233 (2015).
12. N. Lotfian, M. Mirzaei, H. Eshtiagh-Hosseini, et al., Eur. J. Inorg. Chem. **34**, 5908 (2014).
13. L. Parent, P. Oliveira, A. L. Teillout, et al., Inorganics **3**, 341 (2015).
14. H. Xu, L. Li, B. Liu, et al., Inorg. Chem. **48**, 10275 (2009).
15. Z. Luo, P. Kogerler, R. Cao, and C. L. Hill, Inorg. Chem. **48**, 7812 (2009).
16. T. Yamase, H. Abe, E. Ishikawa, et al., Inorg. Chem. **48**, 138 (2009).
17. P. Kögerler, B. Tsukerblat, and A. Müller, Dalton Trans. **39**, 21 (2010).
18. P. Ma, F. Hu, R. Wan, et al., J. Mater. Chem. C **23**, 1 (2016).

19. S. Kuramochi, T. Shiga, J. M. Cameron, et al., Inorganics **5**, 48 (2017).
20. L. S. Zheng, Dalton Trans. **39**, 7588 (2010).
21. S. G. Mitchell and J. M. de la Fuente, J. Mater. Chem. **22**, 18091 (2012).
22. J. E. Mondloch, E. Bayram, and R. G. Finke, J. Mol. Catal. A **355**, 1 (2012).
23. G. A. Barbieri, Mat. Nat. Rend. **23**, 805 (1914).
24. H. Zhang, X. Lin, Y. Yan, and L. Wu, Chem. Commun. **44**, 4575 (2006).
25. M. K. Saini, R. Gupta, S. Parbhakar, et al., RSC Adv. **4**, 25357 (2014).
26. D. Sun, H. Zhang, J. Zhang, et al., J. Solid State Chem. **180**, 393 (2007).
27. T. V. Pinto, D. M. Fernandes, C. Pereira, et al., Dalton Trans. **44**, 4582 (2015).
28. H. X. Liu, F. F. Jian, and J. Wang, Chem. Crystallogr. **40**, 306 (2010).
29. Z. Han, Y. Zhao, J. Peng, et al., J. Solid State Chem. **177**, 4325 (2004).
30. D. G. Allis, R. S. Rarig, E. Burkholder, and J. Zubieta. J. Mol. Struct. **688**, 11 (2004).
31. D. G. Allis, E. Burkholder, and J. Zubieta, Polyhedron **23**, 1145 (2004).
32. B. K. Koo and U. Lee, Inorg. Chim. Acta **359**, 2067 (2006).
33. C. Violaine, D. Remi, B. D. Martine, et al., J. Solid State Chem. **179,** 3615 (2006).
34. M. Najafi, A. Abbasi, M. M. Farahani, and J. Janczak, Dalton Trans. **13**, 34 (2015).
35. K. J. Thorn, A. N. Sarjeant, and A. J. Norquist, Acta Crystallogr. E **61**, m1665 (2005).
36. L. Zhang, Y. Zhao, W. You, et al., J. Cluster Sci. **21**, 93 (2010).
37. B. K. Koo and U. Lee, Inorg. Chim. Acta **359**, 2067 (2006).
38. D. G. Allis, R. S. Rarig, E. Burkholder, and J. Zubieta, J. Mol. Struct. **688**, 11 (2004).
39. D. G. Allis, E. Burkholder, and J. Zubieta, Polyhedron **23**, 1145 (2004).
40. A. C. T. North, D. C. Philips, and F. S. Mathews, Acta Crystallogr. A **24**, 351 (1968).
41. G. M. Sheldrick, Acta Crystallogr. **A 64**, 112 (2008).
42. L. J. Farrugia, J. Appl. Crystallogr. **45**, 849 (2012).
43. I. D. Brown and D. Altermatt, Acta Crystallogr. B **41,** 244 (1985).